Zitierweise:
doi.org/10.1002/anie.202303482

VIP Rare Earth Doped Emitters Very Important Paper

Frenkel Defect-modulated Anti-thermal Quenching Luminescence in Lanthanide-doped $Sc_2(WO_4)_3$

Yang Wei[+], Yue Pan[+], Enlong Zhou, Ze Yuan, Hao Song, Yilin Wang, Jie Zhou, Jiahui Rui, Mengjiao Xu, Lixin Ning, Zhanning Liu, Hongyu Wang, Xiaoji Xie, Xiaobin Tang, Haiquan Su,* Xianran Xing, and Ling Huang**

Abstract: Although large amount of effort has been invested in combating thermal quenching that severely degrades the performance of luminescent materials particularly at high temperatures, not much affirmative progress has been realized. Herein, we demonstrate that the Frenkel defect formed via controlled annealing of $Sc_2(WO_4)_3$:Ln (Ln = Yb, Er, Eu, Tb, Sm), can work as energy reservoir and back-transfer the stored excitation energy to Ln^{3+} upon heating. Therefore, except routine anti-thermal quenching, thermally enhanced 415-fold downshifting and 405-fold upconversion luminescence are even obtained in $Sc_2(WO_4)_3$:Yb/Er, which has set a record of both the Yb^{3+}-Er^{3+} energy transfer efficiency (>85 %) and the working temperature at 500 and 1073 K, respectively. Moreover, this design strategy is extendable to other hosts possessing Frenkel defect, and modulation of which directly determines whether enhanced or decreased luminescence can be obtained. This discovery has paved new avenues to reliable generation of high-temperature luminescence.

Introduction

Lanthanide (Ln^{3+})-doped luminescent materials have been widely engaged in our daily lives ranging from central touchscreen control panel for intelligent homes, advanced anti-counterfeiting, encrypted optical communications, and volumetric displays to wearable healthcare electronics, disease theranostics, subcellular protein manipulation, optogenetics, remote temperature probing, and photo-triggered drug delivery/release.[1–9] Unfortunately, the performance of luminescent materials has been severely degraded by thermal quenching (TQ), which becomes more dominant at elevated temperatures.[10] Many strategies have been developed to circumvent this old yet latest challenge,[11–16] for example, host materials with rigid crystal structures, thermal population, phonon-assistance, desorption of adsorbents and energy compensation from crystal defects represented by point defect including vacancy, interstice atom and substitutional atom in host materials.[17,18] Even though, there has been lack of affirmative principles and unambiguous mechanisms that guide the design of materials for realizing anti-TQ luminescence, particularly at high temperatures.

Herein, we report that Frenkel defect formed in $Sc_2(WO_4)_3$:Ln, i.e., SWO:Ln, via controlled annealing, can serve as energy reservoir and back-transfer the stored excitation energy upon heating, to Ln^{3+}. Thus, anti-TQ, or even thermally enhanced 415-fold downshifting (DSL) and 405-fold upconversion luminescence (UCL) are realized in SWO:Yb/Er, and at a record-high temperature of 500 and 1073 K, respectively. Moreover, this strategy is extendable to other hosts provided that Frenkel defect is formed, modulation of which directly determines the energy supply capability to combat TQ, i.e., observance of enhanced or weakened luminescence.

[*] Dr. Y. Wei,[+] Dr. Y. Pan,[+] Dr. E. Zhou, Dr. Z. Yuan, Dr. H. Song, Dr. Y. Wang, Dr. J. Zhou, J. Rui, Prof. X. Xie, Prof. L. Huang
Institute of Advanced Materials (IAM), Nanjing Tech University
Nanjing, 211816 (China)
E-mail: iamxjxie@njtech.edu.cn
iamlhuang@njtech.edu.cn

M. Xu, Prof. L. Huang
State Kay Laboratory of Chemistry and Utilization of Carbon Based Energy Resources, College of Chemistry, Xinjiang University
Urumqi, 830046 (China)

Dr. Y. Pan,[+] Prof. H. Su
School of Chemistry and Chemical Engineering, Inner Mongolia University
Hohhot, 010021 (China)
E-mail: haiquansu@yahoo.com

Prof. L. Ning
Anhui Key Laboratory of Optoelectric Materials Science and Technology, Department of Physics, Anhui Normal University
Wuhu, Anhui, 241000 (China)

Dr. Z. Liu, X. Xing
Beijing Advanced Innovation Center for Materials Genome Engineering, Institute of Solid-State Chemistry, University of Science and Technology Beijing
Beijing, 100083 (China)

Dr. H. Wang, Prof. X. Tang
Department of Nuclear Science and Technology, Nanjing University of Aeronautics and Astronautics
Nanjing, 211106 (China)

[+] These authors contributed equally to this work.

Results and Discussion

As a classic compound in solid-state chemistry composed of fascinating Sc^{3+} and WO_4^{2-},[19–21] SWO has long been the research focus for luminescent materials,[22,23] solid-state electrolytes,[24,25] negative thermal expansion,[26] infrared transmitting ceramics,[27] and tunable solid-state lasers.[28] These promising functionalities are inherently associated with the critical roles of the highly oxygen-coordinated WO_4 tetrahedra connected with corner-shared ScO_6 octahedra, forming a quasi-layered structure with relatively large interstitial sites. This not only ensures a chemically, thermally, and mechanically stable framework but also favors deviation of partial WO_4^{2-} groups from intrinsic to extrinsic positions during annealing treatment (Figures S1 to S3).

The interactive weight evolution of two Gaussian-deconvoluted emission curves centered at 485 and 550 nm when λ_{ex} increases from 245 to 325 nm (Figure 1a), suggests the existence of two types of emission centers in SWO. Consistently, the relative contribution of two excitation peaks centered at 264 and 297 nm also varies accordingly as the monitored λ_{em} increases from 430 to 700 nm (Figure 1b, Figures S4 and S5). This also well agrees with the mapping results of the excitation and emission intensities of SWO, where two partially overlapped optical centers are clearly

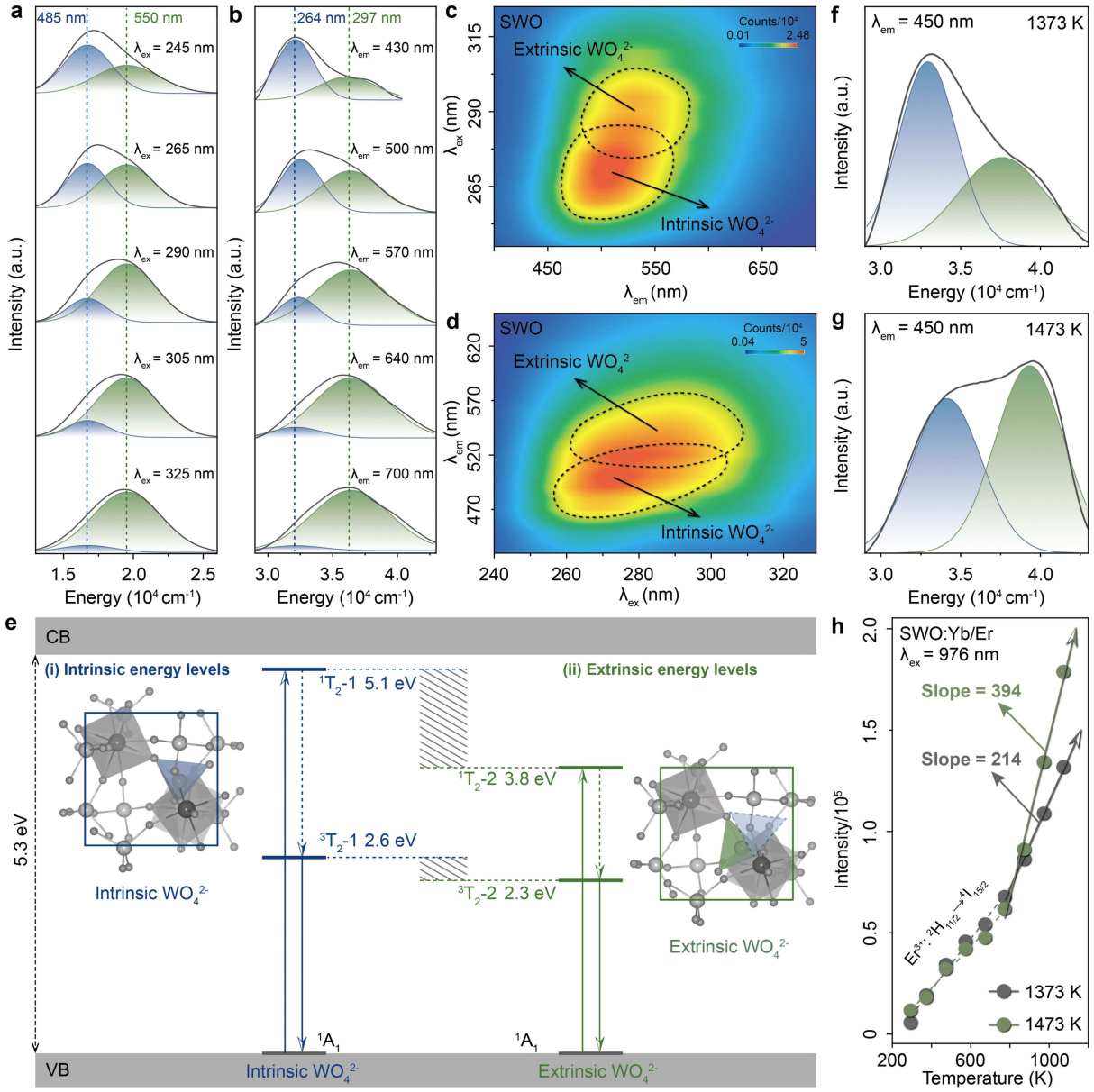

Figure 1. The crystallographic and electronic energy structures of SWO. Wavelength-dependent a) emission and b) excitation spectra of SWO. Mapping result of the c) emission and d) excitation intensity of SWO. e) Band gap structure of SWO showing a quarter of crystallographic cell and energy structure of e(i) intrinsic and e(ii) extrinsic WO_4^{2-}. Excitation spectra of SWO annealed at f) 1373 and g) 1473 K. h) Comparison of luminescence enhancement rate of SWO:Yb/Er annealed at 1373 and 1473 K. Note: Data in (a)–(g) were measured at 77 K.

seen (Figure 1c, d). These two optical centers can be ascribed to the intrinsic and extrinsic WO_4^{2-} groups,[23] respectively, which are regarded as luminescent centers and the excitation is due to the charge transfer (CT) transition of O 2p electrons jumping into the empty W 5d orbits, while emission is generated when CT from W 5d to O 2p occurs.

On the other hand, WO_4^{2-} is apt to deviate from the intrinsic location (blue tetrahedron in Figure 1e(i)) to the interstitial site (green tetrahedron in Figure 1e(ii), Figures S6 and S7) when heated, which forms extrinsic WO_4^{2-}, i.e., the Frenkel defect.[29,30] Hybrid DFT calculations using a $\sqrt{2}\times1\times\sqrt{2}$ supercell (136 atoms) were performed to calculate the formation energy of the extrinsic WO_4^{2-}, and the result (1.35 eV) is quite close to that (1.23 eV) from empirical potential calculations.[30] Moreover, the optimized structure of the extrinsic WO_4^{2-} exhibits a large tetrahedral distortion of $D=0.016$, and only a small $D=0.001$–0.004 for intrinsic WO_4^{2-} [Eq. (S1)]. This means that the crystal field splitting of the W 5d level of the extrinsic WO_4^{2-} should be larger than the intrinsic, leading to lower excitation and emission energies than the intrinsic one. Thus, it is reasonable to ascribe the optical centers at 485/264 and 550/297 nm to intrinsic and extrinsic WO_4^{2-} groups, respectively.

The asymmetric diffuse reflectance spectrum suggests a 5.3 eV optical band gap of SWO (Figure 1e and Figure S8). Calculations following the Planck-Einstein relation [Eq. (S2)] show that intrinsic WO_4^{2-} possesses a singlet $^1T_2$-1 and a triplet $^3T_2$-1 energy level located at 5.1 and 2.6 eV, and accordingly 3.8 and 2.3 eV for the singlet $^1T_2$-2 and triplet $^3T_2$-2 energy levels in extrinsic WO_4^{2-}, respectively. It is exactly such perfect distribution that allows partial overlap of these two groups of energy levels, which forms a singlet and triplet energy reservoir of $^1T_2$-1/$^1T_2$-2 (5.1–3.8 eV) and $^3T_2$-1/$^3T_2$-2 (2.6–2.3 eV) as depicted in the slanted rectangles between Figure 1e(i) and e(ii), respectively.

Energy reservoir stores the excitation energy and releases upon heating, which instead of luminescing, resonantly transfers to Ln^{3+} to combat TQ, and the higher the temperature the more the energy released and transferred. Observance of anti-TQ luminescence is because the amount of energy released exceeds that depleted by TQ, otherwise TQ will dominate. Moreover, the integrated area ratios of the extrinsic and intrinsic WO_4^{2-} groups can be further modulated from 31:69 to 54:46 by increasing the annealing temperature from 1373 to 1473 K (Figure 1f, g). This means more extrinsic WO_4^{2-} groups or Frenkel defects are generated at higher temperature, i.e., larger energy supply capability to combat TQ, as confirmed by the increased slope from 214 to 394 (Figure 1h), using the $^2H_{11/2}\rightarrow{}^4I_{15/2}$ transition of Er^{3+} in SWO:Yb/Er as an example. This is exactly the origin of anti-TQ, or thermally enhanced luminescence discussed below.

Specifically, under excitation at the optimal wavelength of 255 nm, electrons will be first pumped from the ground state $^1A_1$ to the singlet energy reservoir $^1T_2$-1/$^1T_2$-2, which then relax to the triplet energy reservoir $^3T_2$-1/$^3T_2$-2 and finally return to $^1A_1$ accompanied by DSL emission centered at 490 nm (Figure S4b). Alternatively, such energy in $^3T_2$-1/$^3T_2$-2 may be resonantly transferred to matched energy level of $^2F_{5/2}$ in (dual) Yb^{3+}, $^2H_{11/2}$/$^4S_{3/2}$ in Er^{3+}, $^5D_2$ in Eu^{3+}, $^5D_4$ in Tb^{3+}, and $^4I_{11/2}$ in Sm^{3+} (Figure 2a), resulting in host-sensitized DSL at 1053 ($^2F_{5/2}\rightarrow{}^2F_{7/2}$ in Yb^{3+}), 1532 ($^4I_{13/2}\rightarrow{}^4I_{15/2}$ in Er^{3+}, energy relaxed from $^2H_{11/2}$/$^4S_{3/2}$),[3] 613 ($^5D_0\rightarrow{}^7F_2$ in Eu^{3+}),[31] 542 ($^5D_4\rightarrow{}^7F_6$ in Tb^{3+}), and 647 nm ($^4G_{5/2}\rightarrow{}^6H_{9/2}$ in Sm^{3+}), respectively (Figure 2b). Similarly, the triplet energy reservoir can also be directly excited with optimal wavelength at 488 nm, leading to identical resonant energy transfer and DSL emissions of Ln^{3+} (Figure 2c and Figure S9).

As neither Yb^{3+} nor Er^{3+} could be directly excited by 290 nm light, shift of the main emission peak of WO_4^{2-} from 535 to 480 nm in SWO:Yb suggests energy transfer (at 61.4 % efficiency) from WO_4^{2-} to Yb^{3+}, as further validated by both the collapsed dotted-area and the decreased lifetime at 535 nm from 88.6 to 34.2 μs [Figure 2d, Eq. (S3) and Figure S10]. Parallelly, the same dent of dashed lined-area together with the emergence of two characteristic absorption peaks belonging to the $^4F_{7/2}$ (488 nm) and $^2H_{11/2}$ (522 nm)

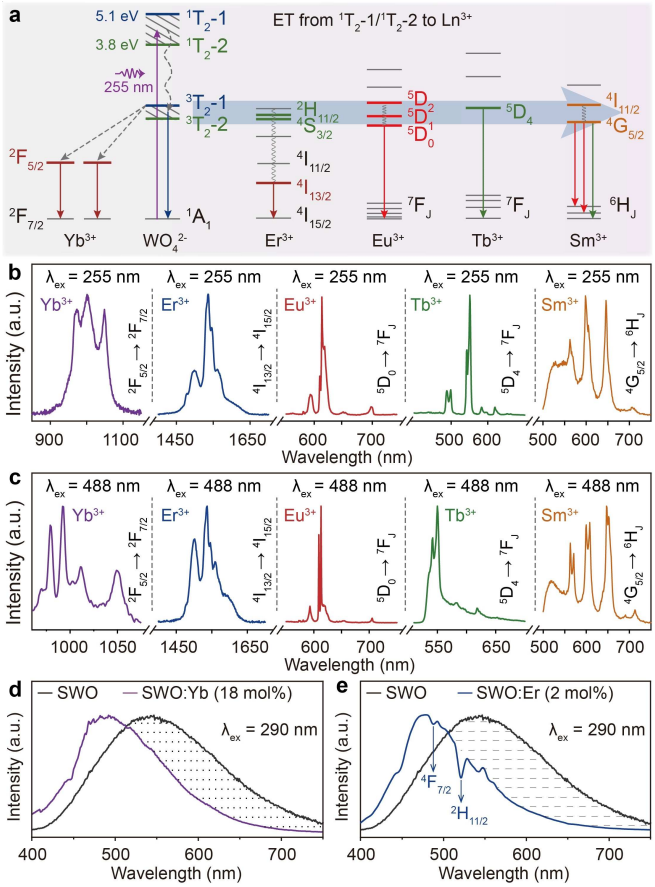

Figure 2. Host-sensitized DSL of SWO:Ln. a) Energy transfer pathways from triplet energy reservoir to Ln^{3+}, prior to which a relaxation from singlet energy reservoir occurs under 255 nm excitation. Host-sensitized DSL of Yb^{3+}, Er^{3+}, Eu^{3+}, Tb^{3+}, and Sm^{3+} under b) 255 and c) 488 nm excitation. Comparison of the emission spectrum of d) SWO versus SWO:Yb and e) SWO versus SWO:Er, which confirms $WO_4^{2-}\rightarrow Yb^{3+}$ and $WO_4^{2-}\rightarrow Er^{3+}$ energy transfer, respectively. Note: Data in (d) and (e) were measured at 77 K.

energy levels in Er^{3+}, as well as the decreased lifetime from 88.6 to 12.8 μs detected in SWO:Er, straightforwardly proves efficient (85.6 %) energy transfer from WO_4^{2-} to Er^{3+} (Figure 2e and Figure S11). This has also reversely rationalized the proposed energy level structures (Figure 1e) and energy transfer pathways (Figure 2a and Figure S9) inside SWO matrix. It is exactly such host-involved high-efficient energy transfer that exceeds that depleted by TQ, and assures significant DSL until 500 K (Figure 3).

As increased amount of energy will be released from singlet and triplet energy reservoirs at elevated temperatures, thermally enhanced DSL shall be expected. Indeed, 9.3-, 2.8-, and 1.4-, 1.6-fold DSL enhancement of Yb^{3+}, Er^{3+} is obtained under excitations at 255 and 488 nm (Figure 3a–d, Figures S12 and S13), respectively. It is also rational to see further 11.8- and 14.6-fold enhancement of Er^{3+} when Yb^{3+} is codoped and consequently decreased 2.5- and 1.2-fold enhancement of Yb^{3+} (Figure 3e–h and Figure S14), respectively, due to the high-efficient Yb^{3+}-Er^{3+} energy transfer.[3] Similarly, instead of normally seen TQ, 3.8-, 1.3-, and 3.1-fold enhanced DSL of Eu^{3+}, Tb^{3+}, and Sm^{3+} is observed under optimal excitations at 464, 498 and 468 nm, respectively (Figure 3i–k and Figure S15). Figure 3l-n lists the optical images of SWO:Eu, SWO:Tb, and SWO:Sm where stable brightness can be seen until 500 K.

In addition to direct excitations of the singlet and triplet energy reservoirs for DSL by light at 255 and 488 nm, respectively, the excited electrons in the $^2F_{5/2}$ level of Yb^{3+} can further absorb 976 nm photons and transfer this energy to the triplet energy reservoir of $^3T_2$-1/$^3T_2$-2 (Figure 4a).

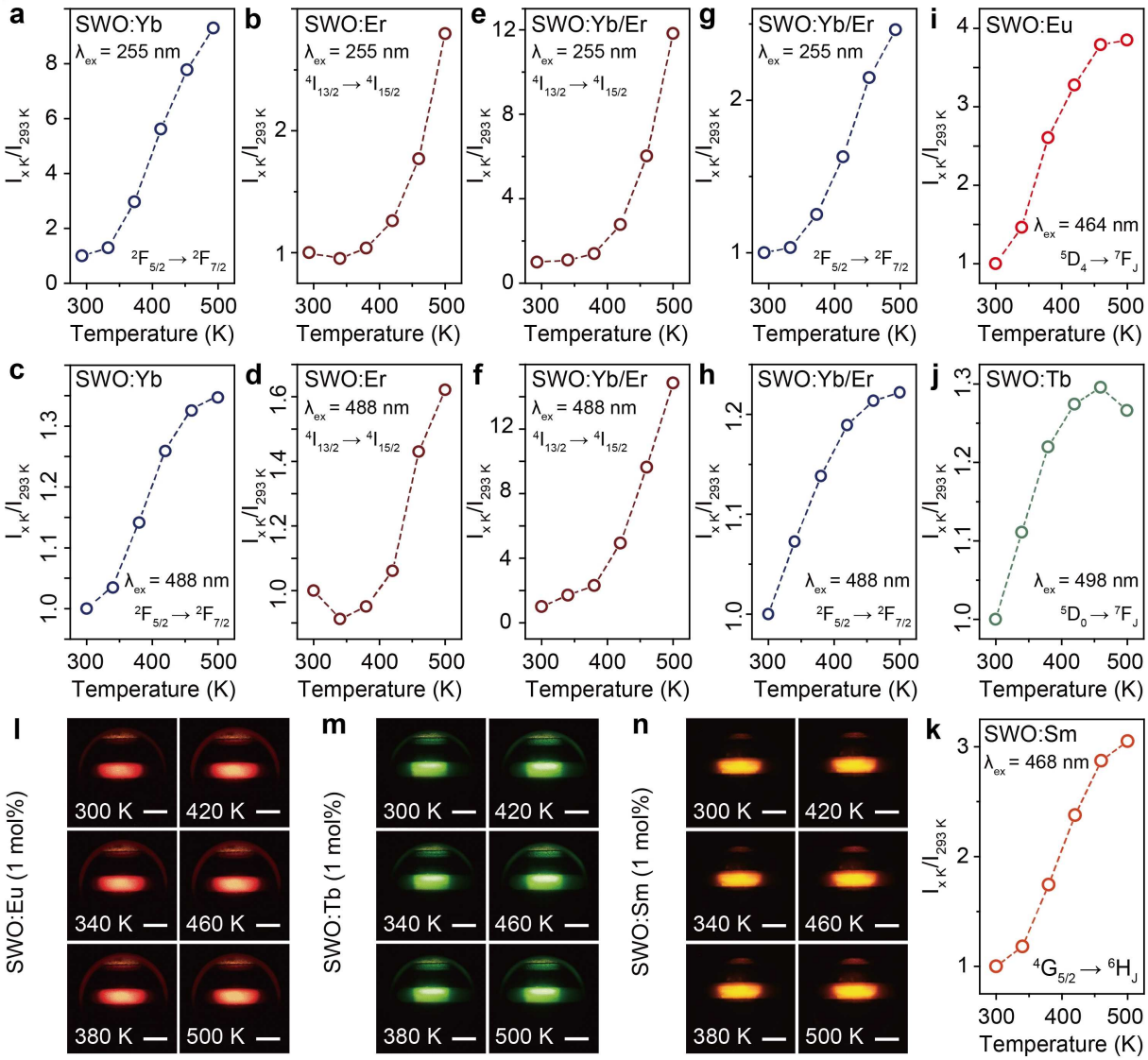

Figure 3. Thermally enhanced DSL of SWO:Ln. Temperature-dependent DSL of a) Yb^{3+} and b) Er^{3+} in SWO under 255 nm excitation, c) Yb^{3+} and d) Er^{3+} in SWO under 488 nm excitation, Er^{3+} in SWO:Yb/Er under e) 255 and f) 488 nm excitations, Yb^{3+} in SWO:Yb/Er under g) 255 and h) 488 nm excitations, as well as i) Eu^{3+} in SWO:Eu, j) Tb^{3+} in SWO:Tb, and k) Sm^{3+} in SWO:Sm, under excitations at 464, 498, and 468 nm, respectively. Optical photographs of l) SWO:Eu, m) SWO:Tb, and n) SWO:Sm show stable brightness at 300–500 K, respectively (scale bar = 3 mm).

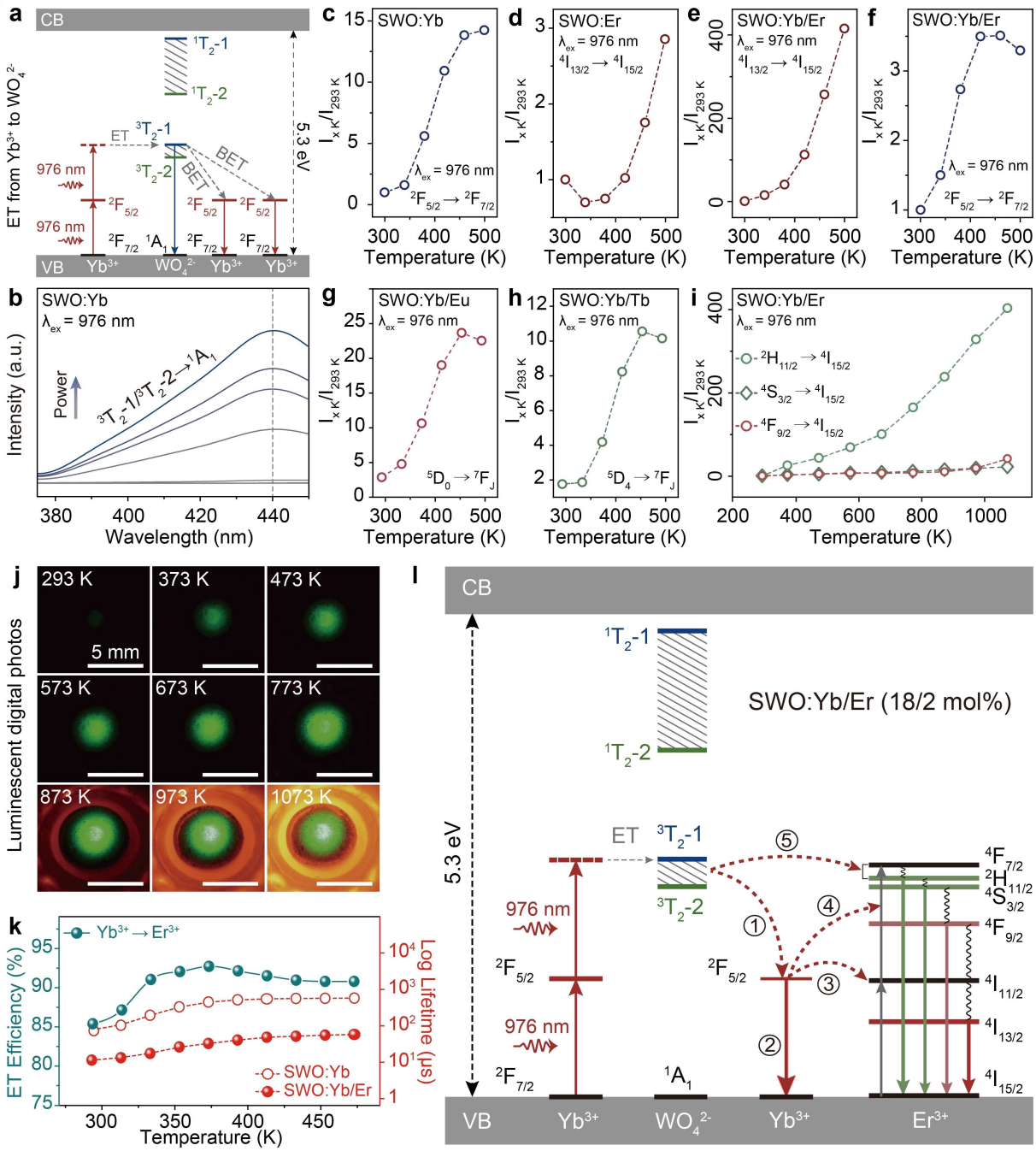

Figure 4. Energy transfer pathways and thermally enhanced luminescence in SWO:Yb/Ln. a) Energy transfer from Yb^{3+} to triplet energy reservoir and back energy transfer (BET) to Yb^{3+}. b) Excitation power-dependent UCL of WO_4^{2-} measured at 5 K. Note: the power density gradually increases from 19.16 to 218.7 W cm^{-2}. Temperature-dependent DSL of c) Yb^{3+} in SWO:Yb, d) Er^{3+} in SWO:Er, e) Er^{3+} and f) Yb^{3+} in SWO:Yb/Er. Temperature-dependent UCL of g) Eu^{3+} in SWO:Yb/Eu, h) Tb^{3+} in SWO:Yb/Tb, and i) Er^{3+} in SWO:Yb/Er. j) In situ photographs of SWO:Yb/Er showing brightness evolution from 293 to 1073 K. k) Temperature-dependent Yb^{3+}-Er^{3+} energy transfer efficiency (green-dotted curve) and lifetime of Yb^{3+} without (red-circled curve) and with Er^{3+} (red-dotted curve). l) Illustration of detailed energy transfer pathways inside SWO:Yb/Er. 976 nm laser was used as excitation source (power density = 4 W cm^{-2}).

This, for the first time, generates host UCL of WO_4^{2-} at 440 nm when electrons return to the ground state of $^1A_1$, as confirmed by the power-dependent emission spectra with excitation power density increasing from 19.16 to 218.7 W cm^{-2} (Figure 4b). Moreover, such energy can also be released upon heating and back transferred to Yb^{3+}, leading to anti-TQ or even thermally enhanced (14.2-fold) DSL of Yb^{3+} at 1053 nm in SWO:Yb under 976 nm excitation and expectedly, 2.8-fold enhanced DSL of Er^{3+} in SWO:Er at 1532 nm following similar pathway (Figure 4c, d, Figures S16 and S17a, b). It is also rational to see further enhanced DSL of Er^{3+} (415.2-fold) and less enhanced DSL

(3.5-fold) of Yb^{3+} in SWO:Er codoped with Yb^{3+} due to the efficient Yb^{3+}-Er^{3+} energy transfer (Figure 4e, f and Figure S17c, d).

On the other hand, the thermally enhanced energy release from triplet energy reservoir, the efficient inter-energy transfer between triplet energy reservoir and Yb^{3+}, as well as the efficient Yb^{3+}-Ln^{3+} energy transfer, form the basis of anti-TQ, or even thermally enhanced UCL of SWO: Yb/Ln. Indeed, 23.4- and 10.5-fold UCL enhancement of Eu^{3+} and Tb^{3+} are obtained at temperatures up to 500 K (Figure 4g, h and Figure S18), which used to be hardly achieved even at room temperature due to the poor energy level match with Yb^{3+}. Furthermore, a 405.3-, 22.7-, and 42.2-fold UCL enhancement of Er^{3+} at emissions of 522, 548, and 657 nm is seen in Figure 4i, respectively. Observance of the rapidly brightened green dot at 293–1073 K and its regularly blinking at 1073 K induced by the periodically controlled on/off of the 976 nm laser (Figure 4j, Videos S1 and S2) have unambiguously confirmed a typical UCL process. Moreover, the 85–90 % Yb^{3+}-Er^{3+} energy transfer efficiency remains so far the record value compared with that of 21 % in the most studied $NaYF_4$:Yb/Er [Figure 4k, Figures S19, S20, Eq. (S3) and Table S1].

As illustrated in Figure 4l, the triplet energy reservoir first receives energy from Yb^{3+} under 976 nm excitation, then the increasingly released energy upon heating may have the following Routes to go: 1) back-transfer to Yb^{3+} leading to enhanced DSL of Yb^{3+} (Figure 4c) following Routes (1) and (2), 2) transfer to the energy level of $^4I_{11/2}$ in Er^{3+} causing enhanced DSL in SWO:Yb/Er (Figure 4e) following Routes (1) and (3), 3) transfer to $^4I_{11/2}$ and $^2H_{11/2}$/$^4S_{3/2}$ in Er^{3+} resulting in enhanced UCL (Figure 4i) following Routes (1), (3), and (4), and 4) directly transfer to $^2H_{11/2}$/$^4S_{3/2}$ in Er^{3+} following Route (5), leading to enhanced DSL and decreased UCL in SWO:Er (Figure 4d and Figure S21). We would like to point out that, the triplet energy reservoir supplies much less energy to Er^{3+} than that depleted by TQ in the absence of Yb^{3+} (Route (5)), which explains why only small DSL enhancement and decreased UCL of Er^{3+} is observed in SWO:Er, respectively. Thus, the enhanced DSL and UCL in Yb^{3+} codoped SWO:Er (Figure 4e, i) contains the contribution from Route (5), though very little. This also proves that although the energy reservoir is very powerful in supplying energy to combat TQ, codoped Yb^{3+} plays an irreplaceable role for such giant enhancement.

In addition, our calculations have further shown that, the shortened Yb^{3+}-Er^{3+} distance (from 11.46 to 11.42 Å) caused by negative thermal expansion (NTE) only contributes very little to UCL in SWO:Yb/Er [Eqs. (S4), (S5) and Table S2],[32–35] which is far insufficient to account for the giant enhancement seen in Figure 4i. Meanwhile, the distortion index of Er^{3+} site only increases from 0.019 to 0.034, which also suggests negligible contribution of NTE to such giant enhancement (Table S3 and Figure S22).

It is worth emphasizing that: i) this is the first case of activator (Yb^{3+})-sensitized UCL of host (SWO), ii) the energy reservoir is so powerful that TQ can be easily overcome, iii) giant anti-TQ luminescence is realized, iv) under multiple wavelength excitations (255 and 488 nm for SWO, 976 nm for Ln^{3+}), and v) the >85 % Yb^{3+}-Er^{3+} energy transfer efficiency has set a record. Compared with previously reported anti-TQ luminescence due to energy compensation from isolated point defects,[11,12] the systematically generated Frenkel defect via controlled annealing crosses the entire crystallographic framework of SWO. This imparts SWO very strong energy supply capability to combat TQ, which might explain why instead of anti-TQ, enhanced luminescence even at high-temperature can be realized.

Moreover, such enhancement can be obtained not only in SWO, but also in its analogues, orthorhombic $Lu_2(WO_4)_3$: Yb/Er, as long as the Frenkel defect, i.e., energy reservoir, can form (Figure S23). As a stark contrast, monoclinic $Gd_2(WO_4)_3$ possesses a crowded lattice composed of both corner and edge-shared GdO_8 dodecahedra and WO_4 tetrahedra, which doesn't favor deviation of WO_4^{2-} from the intrinsic location, i.e., formation of Frenkel defect. This well agrees with the single excitation and emission peak at 302 and 500 nm, respectively. Thus, there is no energy reservoir formation, so that the energy back-transfer is cut off, leading to monotonous TQ luminescence (Figures S24–S26).

The efficient SWO↔Yb^{3+} energy transfer and the multi-overlapped absorption bands with the sunlight in SWO:Yb/Ln at UV (245–325 nm for singlet energy reservoir), visible (485–550 nm for triplet energy reservoir), and NIR (855–1100 nm for Yb^{3+} and Er^{3+}), are highly promising for solar energy harvesting (Figure 5a, b) when integrated with thermophotovoltaic cell (TPVC), particularly when the rich UV irradiation in outer space is considered.[36–38]

Indeed, a larger short-circuit current (Isc) increase from 13.4 to 15.2 mA at 293–1073 K together with a 36.6-fold improvement ($\Delta Isc_x/\Delta Isc_1$) is seen in SWO:Yb/Er-InGaAs TPVC at 1073 K under 976 nm excitation, compared with those of 4.09 to 4.54 mA and 9.0-fold improvement in SWO: Er- InGaAs TPVC (Figure 5c, d and Figures S27–S29), respectively. Similarly, under 488 nm excitation, the increases of Isc from 1.64 to 1.69 mA and 6.8-fold improvement in SWO:Yb/Er-InGaAs TPVC is superior to those from 1.26 to 1.29 mA and 3.9-fold improvement in SWO:Er-InGaAs TPVC (Figure 5e, f and Figure S30), respectively. More intriguingly, the Isc of green emission-responsive SWO:Yb/Er-GaAs TPVC increases from 2.08 to 2.74 μA together with a 246-fold improvement at 1073 K, while that of SWO:Er-GaAs decreases due to TQ (Figure 5g, h, Figures S31 and S32).

Conclusion

We have explicitly demonstrated that modulation of the $Sc_2(WO_4)_3$-type host determines both the formation and amount of Frenkel defect, which directly associates with anti-TQ capability, i.e., enhanced or decreased luminescence. This study has enriched the luminescence mechanism studies, and updated the solid-state chemical principles of the old yet charming SWO,[24,39] i.e., the unique role of WO_4^{2-}. More importantly, this work has pointed out a new direction to material design for reliable generation of high-

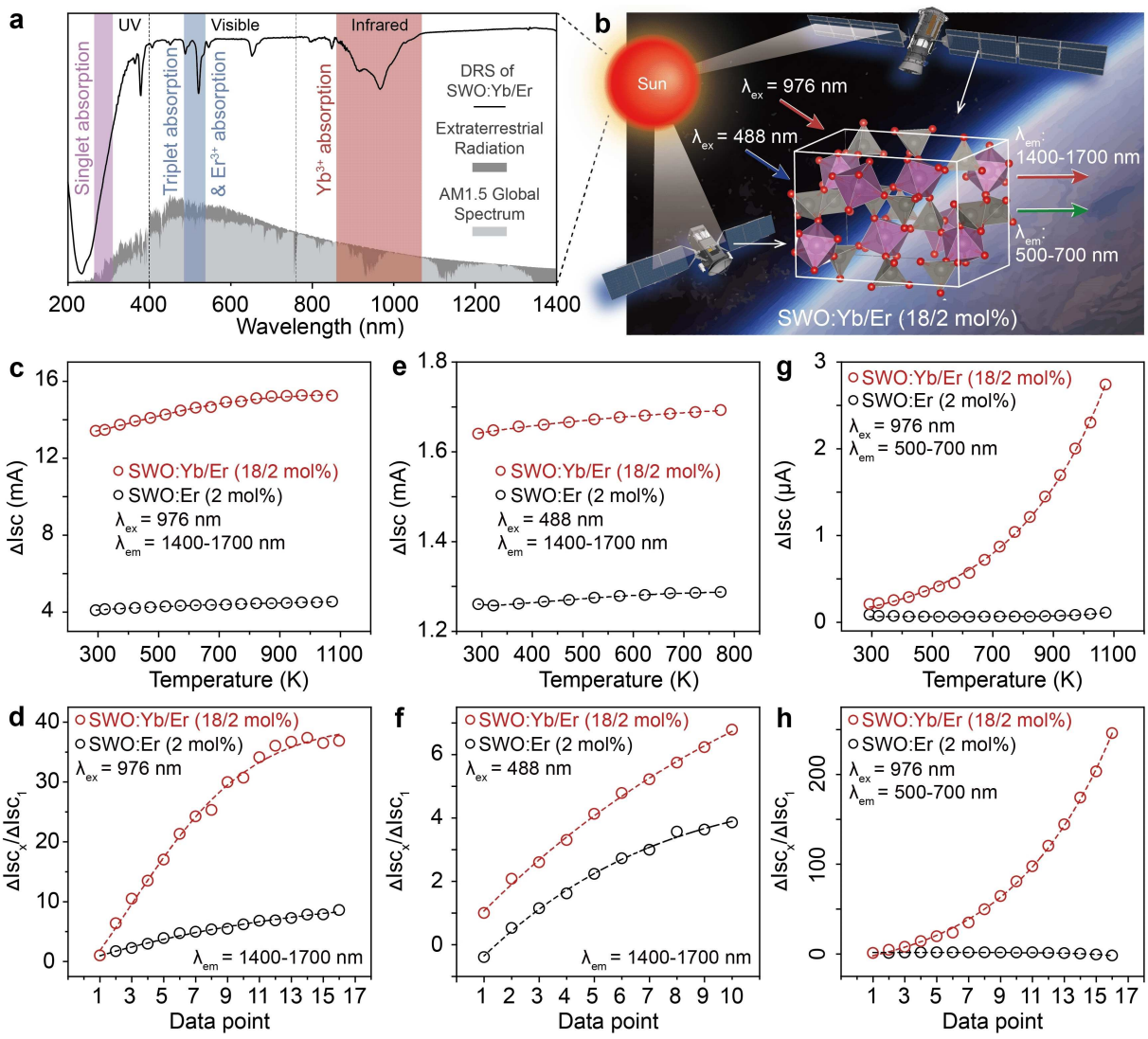

Figure 5. Application of thermally enhanced DSL and UCL in TPVC. a) Overlap of the optical absorption of SWO:Yb/Er with solar spectrum. b) Schematic diagram of SWO:Yb/Er-based TPVC for solar energy harvesting in outer space. c) Temperature-dependent Isc of respective TPVC by utilizing NIR emission of Er^{3+} under 976 nm excitation (power density: 4 W cm^{-2}) and d current intensity ratio $\Delta Isc_x/\Delta Isc_1$ at different temperature interval. (ΔIsc_1: 293–323 K, ΔIsc_2: 323–373 K, etc.). e) Temperature-dependent Isc of respective TPVC by utilizing NIR emission of Er^{3+} under 488 nm excitation (power density: 0.6 W cm^{-2}) and f current intensity ratio $\Delta Isc_x/\Delta Isc_1$ at different temperature interval. g) Temperature-dependent Isc of respective TPVC by utilizing visible emissions of Er^{3+} under 976 nm excitation (power density: 4 W cm^{-2}) and h current intensity ratio $\Delta Isc_x/\Delta Isc_1$ at different temperature interval.

temperature luminescence, which possesses great potentials in high-power lighting, high-power lasing, fracture probing in engine blades, thermophotovoltaics, photothermal catalysis, and so on.

Acknowledgements

Funding: This work was supported by the National Natural Science Foundation of China (Grant nos. 21871137 and 91956107).

Conflict of Interest

The authors declare no conflict of interest.

Data Availability Statement

The data that support the findings of this study are available in the Supporting Information of this article.

Keywords: Downshifting Luminescence · Energy Transfer · Frenkel Defect · Thermal Quenching · Upconversion Luminescence

[1] G. Blasse, B. C. Grabmaier, *Luminescent Materials*, Springer Berlin Heidelberg, Berlin, **1994**.
[2] A. Kital, *Luminescent Materials and Applications*, Wiley, Hoboken, **2008**, p. 294.
[3] X. Cheng, J. Zhou, J. Yue, Y. Wei, C. Gao, X. Xie, L. Huang, *Chem. Rev.* **2022**, *122*, 15998–16050.
[4] X. Liu, Y. Wang, X. Li, Z. Yi, R. Deng, L. Liang, X. Xie, D. T. B. Loong, S. Song, D. Fan, A. H. All, H. Zhang, L. Huang, X. Liu, *Nat. Commun.* **2017**, *8*, 899.
[5] S. Chen, A. Z. Weitemier, X. Zeng, L. He, X. Wang, Y. Tao, A. Huang, Y. Hashimotodani, M. Kano, H. Iwasaki, L. K. Parajuli, S. Okabe, D. B. Teh, A. H. All, I. Tsutsui-Kimura, K. F. Tanaka, X. Liu, T. J. McHugh, *Science* **2018**, *359*, 679–684.
[6] T. Hartman, R. G. Geitenbeek, G. T. Whiting, B. M. Weckhuysen, *Nat. Catal.* **2019**, *2*, 986–996.
[7] C. D. S. Brites, S. Balabhadra, L. D. Carlos, *Adv. Opt. Mater.* **2019**, *7*, 1801239.
[8] S. Xie, Y. Du, Y. Zhang, Z. Wang, D. Zhang, L. He, L. Qiu, J. Jiang, W. Tan, *Nat. Commun.* **2020**, *11*, 1347.
[9] S. N. Sanders, T. H. Schloemer, M. K. Gangishetty, D. Anderson, M. Seitz, A. O. Gallegos, R. C. Stokes, D. N. Congreve, *Nature* **2022**, *604*, 474–478.
[10] D. J. Robbins, B. Cockayne, J. L. Glasper, B. Lent, *J. Electrochem. Soc.* **1979**, *126*, 1213–1220.
[11] Y. H. Kim, P. Arunkumar, B. Kim, S. Unithrattil, E. Kim, S. Moon, J. Y. Hyun, K. H. Kim, D. Lee, J. Lee, W. B. Im, *Nat. Mater.* **2017**, *16*, 543–550.
[12] J. Qiao, L. Ning, M. S. Molokeev, Y. Chuang, Q. Liu, Z. Xia, *J. Am. Chem. Soc.* **2018**, *140*, 9730–9736.
[13] W. Xu, Y. Hu, L. Zheng, Z. Zhang, W. Cao, H. Liu, X. Wu, *J. Lumin.* **2019**, *208*, 415–423.
[14] J. Zhou, S. Wen, J. Liao, C. Clarke, S. A. Tawfik, W. Ren, C. Mi, F. Wang, D. Jin, *Nat. Photonics* **2018**, *12*, 154–158.
[15] Y. Hu, Q. Shao, P. Zhang, Y. Dong, F. Fang, J. Jiang, *J. Phys. Chem. C* **2018**, *122*, 26142–26152.
[16] D. Li, W. Wang, X. Liu, C. Jiang, J. Qiu, *J. Mater. Chem. C* **2019**, *7*, 4336–4343.
[17] J. Qiao, S. Zhang, X. Zhou, W. Chen, R. Gautier, Z. Xia, *Adv. Mater.* **2022**, *34*, 2201887.
[18] X. Zhou, L. Ning, J. Qiao, Y. Zhao, P. Xiong, Z. Xia, *Nat. Commun.* **2022**, *13*, 7589.
[19] J. Røyset, N. Ryum, *Int. Mater. Rev.* **2005**, *50*, 19–44.
[20] B. F. Sels, D. E. Vos, M. Buntinx, F. Pierard, A. K. Mesmaeker, P. A. Jacobs, *Nature* **1999**, *400*, 855–857.
[21] X. Teng, Y. Zhu, W. Wei, S. Wang, J. Huang, R. Naccache, W. Hu, A. I. Tok, Y. Han, Q. Zhang, Q. Fan, W. Huang, J. A. Capobianco, L. Huang, *J. Am. Chem. Soc.* **2012**, *134*, 8340–8343.
[22] H. J. Borchardt, *J. Chem. Phys.* **1963**, *39*, 504.
[23] G. Blasse, M. Ouwerkerk, *J. Electrochem. Soc.* **1980**, *127*, 429.
[24] G. Adachi, N. Imanaka, S. Tamura, *Chem. Rev.* **2002**, *102*, 2405–2430.
[25] Y. H. Kobayashi, T. Egawa, S. Tamura, N. Imanaka, G. Adachi, *Chem. Mater.* **1997**, *9*, 1649–1654.
[26] J. S. O. Evans, T. A. Mary, A. W. Sleight, *J. Solid State Chem.* **1998**, *137*, 148–160.
[27] D. N. Dasgupta, E. Sörge, B. Butler, T. Wen, D. K. Shetty, L. R. Cambrea, D. C. Harris, *J. Mater. Sci.* **2012**, *47*, 6286–6296.
[28] A. Yordanova, R. Iordanova, I. Koseva, V. Nikolov, R. Kukeva, *Luminescence* **2018**, *33*, 1185–1193.
[29] Y. Zhou, S. Adams, R. P. Rao, D. D. Edwards, A. Neiman, N. Pestereva, *Chem. Mater.* **2008**, *20*, 6335–6345.
[30] Y. Zhou, R. P. Rao, S. Adams, *Solid State Ionics* **2011**, *192*, 34–37.
[31] J. C. Boyer, F. Vetrone, J. A. Capobianco, A. Speghini, M. Bettinelli, *J. Phys. Chem. B* **2004**, *108*, 20137–20143.
[32] T. Kushida, *J. Phys. Soc. Jpn.* **1973**, *34*, 1318–1326.
[33] O. L. Malta, *J. Non-Cryst. Solids* **2008**, *354*, 4770–4776.
[34] T. Förster, *Radiat. Res. Suppl.* **1960**, *2*, 326–339.
[35] A. N. Carneiro Neto, R. T. Moura, Jr., A. Shyichuk, V. Paterlini, F. Piccinelli, M. Bettinelli, O. L. Malta, *J. Phys. Chem. C* **2020**, *124*, 10105–10116.
[36] B. S. Richards, D. Hudry, D. Busko, A. Turshatov, I. A. Howard, *Chem. Rev.* **2021**, *121*, 9165–9195.
[37] Z. Dong, W. Li, H. Wang, X. Jiang, H. Liu, L. Zhu, H. Chen, *Sol. RRL* **2021**, *5*, 2100370.
[38] A. Manor, N. Kruger, T. Sabapathy, C. Rotschild, *Nat. Commun.* **2016**, *7*, 13167.
[39] T. A. Mary, J. S. O. Evans, T. Vogt, A. W. Sleight, *Science* **1996**, *272*, 90–92.
[40] J. Heyd, G. Scuseria, M. Ernzerhof, *J. Chem. Phys.* **2003**, *118*, 8207.
[41] A. Krukau, O. Vydrov, A. Izmaylov, G. Scuseria, *J. Chem. Phys.* **2006**, *125*, 224106.
[42] G. Kresse, J. Furthmüller, *Phys. Rev. B* **1996**, *54*, 11169.
[43] G. Kresse, D. Joubert, *Phys. Rev. B* **1999**, *59*, 1758.
[44] P. E. Blöchl, *Phys. Rev. B* **1994**, *50*, 17953.
[45] P. Kubelka, F. Munk, *Z. Tech. Phys.* **1931**, *12*, 593–609.
[46] J. R. Lakowicz, *Principles of Fluorescence Spectroscopy*, Springer, New York, **2006**.
[47] A. Bednarkiewicz, M. Nyk, M. Samoc, W. Strek, *J. Phys. Chem. C* **2010**, *114*, 17535–17541.
[48] A. N. Carneiro Neto, R. T. Moura Jr, O. L. Malta, *J. Lumin.* **2019**, *210*, 342–347.
[49] X. Qin, A. N. Carneiro Neto, R. L. Longo, Y. Wu, O. L. Malta, X. Liu, *J. Phys. Chem. Lett.* **2021**, *12*, 1520–1541.
[50] V. Trannoy, A. N. Carneiro Neto, C. D. S. Brites, L. D. Carlos, H. Serier, *Adv. Opt. Mater.* **2021**, *9*, 2001938.

Manuscript received: March 8, 2023
Accepted manuscript online: May 2, 2023
Version of record online: ■■, ■■

Forschungsartikel

Rare Earth Doped Emitters

Y. Wei, Y. Pan, E. Zhou, Z. Yuan, H. Song, Y. Wang, J. Zhou, J. Rui, M. Xu, L. Ning, Z. Liu, H. Wang, X. Xie,* X. Tang, H. Su,* X. Xing, L. Huang* e202303482

Frenkel Defect-modulated Anti-thermal Quenching Luminescence in Lanthanide-doped $Sc_2(WO_4)_3$

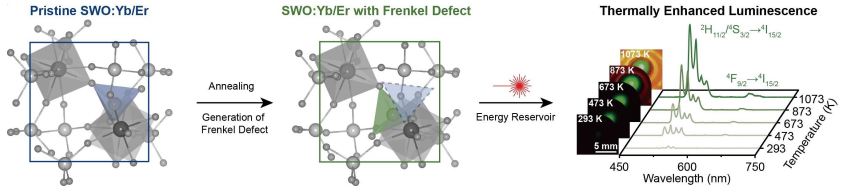

Upon heating, deviation from intrinsic to extrinsic position of partial WO_4^{2-} in $Sc_2(WO_4)_3$:Ln forms Frenkel defect, which serves as energy reservoir and back-transfers the stored excitation energy to Ln^{3+} so that thermally enhanced downshifting and upconversion luminescence at record-high working temperature of 500 and 1073 K are obtained, respectively.